OPTICS

Ultrafast optical ranging using microresonator soliton frequency combs

P. Trocha,[1]* M. Karpov,[2]* D. Ganin,[1]* M. H. P. Pfeiffer,[2] A. Kordts,[2] S. Wolf,[1] J. Krockenberger,[1] P. Marin-Palomo,[1] C. Weimann,[1]† S. Randel,[1,3] W. Freude,[1,3] T. J. Kippenberg,[2]‡ C. Koos[1,3]‡

Light detection and ranging is widely used in science and industry. Over the past decade, optical frequency combs were shown to offer advantages in optical ranging, enabling fast distance acquisition with high accuracy. Driven by emerging high-volume applications such as industrial sensing, drone navigation, or autonomous driving, there is now a growing demand for compact ranging systems. Here, we show that soliton Kerr comb generation in integrated silicon nitride microresonators provides a route to high-performance chip-scale ranging systems. We demonstrate dual-comb distance measurements with Allan deviations down to 12 nanometers at averaging times of 13 microseconds along with ultrafast ranging at acquisition rates of 100 megahertz, allowing for in-flight sampling of gun projectiles moving at 150 meters per second. Combining integrated soliton-comb ranging systems with chip-scale nanophotonic phased arrays could enable compact ultrafast ranging systems for emerging mass applications.

Laser-based light detection and ranging (LIDAR) is a key technology in industrial and scientific metrology, offering high-precision, long-range, and fast acquisition (*1*, *2*). LIDAR systems have found their way into a wide variety of applications, comprising, for example, industrial process monitoring, autonomous driving, satellite formation flying, or drone navigation. When it comes to fast and accurate ranging over extended distances, optical frequency combs (*3*) have been demonstrated to exhibit characteristic advantages, exploiting time-of-flight (TOF) schemes (*4*), interferometric approaches (*5*), or combinations thereof (*6*). In early experiments (*4*), mode-locked fiber lasers were used for TOF ranging, thereby primarily exploiting the stability of the repetition rate. Regarding interferometric schemes, optical frequency combs were exploited to stabilize the frequency interval between continuous-wave (CW) lasers used in synthetic-wavelength interferometry (*5*, *7*). Dual-comb schemes, which rely on multiheterodyne detection by coherent superposition of a pair of slightly detuned frequency combs (*8*), allow combining of TOF measurements with optical interferometry, thereby simultaneously exploiting the radio-frequency coherence of the pulse train and the optical coherence of the individual comb tones (*6*). More recently, comb-based schemes have been demonstrated as a viable path to high-speed sampling with acquisition times down to 500 ns (*9*).

However, besides accuracy and acquisition speed, footprint is becoming increasingly important for LIDAR systems. On the technology side, recent advances in photonic integration show that large-scale nanophotonic phased arrays (*10*, *11*) open a promising path toward ultracompact systems for rapid high-resolution beam steering. To harness the full potential of these approaches, the optical phased arrays need to be complemented by LIDAR engines that combine high precision with ultrafast acquisition and that are amenable to chip-scale integration. Existing dual-comb LIDAR concepts cannot fulfill these requirements because they rely either on cavity-stabilized mode-locked fiber lasers (*6*) or on spectral broadening of initially narrowband seed combs (*9*), which typically require delicate fiber-based dispersion management schemes, usually in combination with intermediate amplifiers.

Here, we show that dissipative Kerr soliton (DKS) states (*12*, *13*) in microresonator-based optical frequency combs (*14*, *15*) provide a route to integrated LIDAR systems that combine subwavelength accuracy and unprecedented acquisition speed with scalable fabrication, robust implementation, and compact form factors. DKSs are solutions of a driven, damped, and detuned nonlinear Schrödinger equation, often referred to as a Lugiato-Lefever equation (*16*). Such ultrashort temporal solitons can circulate continuously in the cavity, relying on a double balance of dispersion and nonlinearity as well as parametric gain and cavity loss (*13*). In the frequency domain, DKS pulse trains correspond to optical frequency combs, which combine large bandwidths and smooth spectral envelopes with free spectral ranges in the range from tens of gigahertz to a few terahertz. Microresonator-based DKSs have recently been used in low-noise microwave generation (*17*), frequency metrology (*18*), dual-comb spectroscopy (*19*), coherent communications (*20*), and optical frequency synthesis (*21*). In our demonstrations, we exploit DKS combs for synthetic-wavelength interferometry with massively parallel multiheterodyne detection. Our scheme is based on a pair of free-running comb generators and does not require phase locking of the combs to each other. The large optical bandwidth of more than 11 THz leads to highly precise distance measurements with Allan deviations reaching 12 nm at an averaging time of 14 μs, whereas the large free spectral range (FSR) enables high-speed measurements at rates of up to 100 MHz. We prove the viability of our technique by sampling the naturally scattering surface of air-gun projectiles on the fly, achieving lateral spatial resolutions of more than 2 μm for object speeds of more than 150 m/s.

For DKS comb generation, we use a pair of CW-pumped silicon nitride (Si_3N_4) microring resonators on separate chips (*22*–*24*). The devices (Fig. 1A) are fabricated using the photonic Damascene process (*25*), which enables crack-free fabrication of high-quality (Q) microresonators (Q > 1 million) with large waveguide dimensions (1.65 by 0.85 μm). DKS comb generation is achieved by sweeping the pump laser frequency from the effectively blue-detuned to a defined point in the effectively red-detuned regime of a selected cavity resonance, where the microresonator system supports soliton formation (*13*) (Fig. 1B). Once the laser scan stops, typically a multisoliton state is generated. By next applying the backward frequency tuning technique (*26*), a single-soliton state corresponding to an optical frequency comb with a spectrally smooth squared hyperbolic secant ($sech^2$) shape envelope (Fig. 1C) is achieved in a deterministic manner. A more detailed description of the experimental setup and of the microresonator devices can be found in (*27*).

The experimental setup used for dual-comb ranging is depicted in Fig. 2A. For multiheterodyne detection, we use two Kerr comb generators with slightly different free spectral ranges of $\omega_{S,r}/2\pi$ = 95.842 GHz and $\omega_{LO,r}/2\pi$ = 95.746 GHz, respectively. To demonstrate that our concept does not require phase locking of the DKS combs, we used a pair of free-running CW lasers to pump the microresonators and compensate for the stochastic phase drifts by digital signal processing (*27*). The pump light for the signal and the Local oscillator (LO) comb is amplified by erbium-doped fiber amplifiers (EDFA) to power levels of 3.5 and 2.6 W, respectively, and then coupled to the microresonator chips with a coupling efficiency of ~60% per facet. The resulting combs feature overall power levels of 4.3 and 2.5 mW and are amplified by a pair of C+L–band (1530 to

[1]Institute of Photonics and Quantum Electronics (IPQ), Karlsruhe Institute of Technology (KIT), 76131 Karlsruhe, Germany. [2]Laboratory of Photonics and Quantum Measurements (LPQM), École Polytechnique Fédérale de Lausanne (EPFL), CH-1015 Lausanne, Switzerland. [3]Institute of Microstructure Technology (IMT), Karlsruhe Institute of Technology, 76131 Karlsruhe, Germany.
*These authors contributed equally to this work. †Present address: Corporate Research and Technology, Carl Zeiss AG, Oberkochen, Germany. **‡Corresponding author. Email: tobias.kippenberg@epfl.ch (T.J.K.); christian.koos@kit.edu (C.K.)**

1565 nm and 1565 to 1625 nm) EDFA to 450 mW to improve the measurement accuracy. A spectrum of an amplified comb is shown in Fig. 2C. The gain bandwidth of the EDFA limits the number of usable lines to about 115, which is sufficient for our experiments.

For distance measurements, the signal comb is split by a fiber-based 50:50 coupler, and one part is routed to the target and back to a balanced measurement photodetector (meas. PD), while the other part is directly sent to the balanced reference detector (ref. PD); see Fig. 2A. Measurement and reference PDs feature bandwidths of 43 GHz. Similarly, the LO comb is split into two portions, which are routed to the measurement PD and the reference PD for multiheterodyne detection. The resulting baseband signal contains discrete beat notes, which are recorded by a 33-GHz real-time sampling oscilloscope and separated by means of a numerically calculated Fourier transform. The distance to the target is extracted from the phase of the baseband beat notes. Data processing and evaluation are performed offline; see (*27*) for details of the underlying algorithms.

Figure 2B shows the Fourier transform of a recorded baseband signal, revealing the various beat notes between the signal and LO comb lines. The spacing of the beat notes is given by the difference of the line spacing of the LO and the signal comb and amounts to $\Delta f_r = \Delta\omega_r/2\pi$ = 96.4 MHz, thereby dictating a minimum possible acquisition time of $T_{\min} = 1/\Delta f_r$ = 10.4 ns and a maximum possible distance acquisition rate of 96.4 MHz.

For a thorough stability and precision analysis of our dual-comb scheme, we measure the distance to a static mirror and evaluate the Allan deviation. The entire measurement contains a series of ~1.1×10^6 individual data points taken at an acquisition time of 10.4 ns per point, leading to a total duration of ~12 ms. The extracted Allan deviation is plotted in Fig. 2D. At an averaging time of 10.4 ns, the Allan deviation amounts to 284 nm, and it decreases to 12 nm for an averaging time of 13 μs. At small averaging times, the Allan deviation decreases with increasing averaging time, as expected for dominating white noise such as shot noise or amplified spontaneous emission (ASE) originating from the EDFA. For larger averaging times, the Allan deviation increases, which we attribute to thermal drift of the fibers and to mechanical vibrations at acoustic frequencies. The current measurement accuracy is hence only limited by a nonideal implementation of the system. Further improvements are possible by reducing the ASE noise floor of the EDFA and by avoiding thermal drift and mechanical vibrations. Fundamentally, the measurement accuracy is only limited by ineviable shot noise and possibly by additional ASE noise of ideal EDFA. For comb powers of 10 mW, this would allow for measurement accuracies of better than 10 nm at the highest acquisition rate of 100 MHz; see (*27*) for details.

Besides the Allan deviation, we also estimated the accuracy of our technique by measuring variable distances to a target that is moved over a full ambiguity distance $L_{\mathrm{amb}} = \frac{c}{2}\frac{2\pi}{\omega_{\mathrm{S,r}}}$ (Fig. 2E). In this experiment, the target mirror is stepped in increments of 50 μm using a feedback-stabilized stage with a positioning accuracy of more than 50 nm. To reduce the impact of fiber drift, the distance measurement is continuously switched between the movable target mirror and a static calibration mirror in quick succession, taking between 6500 and 9500 measurements with the full acquisition rate of ~96 MHz on each mirror; see (*27*). From these measurements, we extract the distance to the target mirror and the associated standard deviation; see (*27*) for details. In the upper part of Fig. 2E, the measured distance is plotted as a function of the distance set by the translation state. Measured distances exceeding the ambiguity distance of L_{amb} = 1.56 mm are unwrapped manually. The bottom part of Fig. 2E shows the residual deviations of the measured positions from the set positions along with the respective standard deviations indicated as error bars. Importantly, no cyclic error is observed throughout the ambiguity distance. We determine the accuracy of our measurement to 188 nm, defined as the standard deviation of the residuals, which are of the same order of magnitude as the 50-nm positioning accuracy of the stage specified by the manufacturer. In this measurement, the refractive index of air is considered according to Ciddor's formula for ambient laboratory conditions. The measured 188-nm standard deviation of the residuals is still dominated by drift and acoustic vibrations of the measurement setup rather than by the measurement system itself, despite compensation via the static calibration mirror. This can be inferred from the fact that the standard deviation of 188 nm is still much larger than the intrinsic system-related errors of 5 nm that should be expected for the averaging time of 100 μs; see (*27*) for a more detailed discussion.

To validate the reproducibility of our system and to benchmark the results with respect to existing techniques, we measured the profile of a quickly rotating disk with grooves of different depths on its surface (see Fig. 3A). In this experiment, the measurement beam is focused to the surface near the edge of the disk, which rotates at a frequency of about 600 Hz, thus resulting in an edge velocity of 160 m/s. The distance acquisition rate in this experiment amounts to 96.5 MHz, limited by the spectral spacing of $\Delta\omega_r/2\pi$ of the beat notes in the baseband photocurrent but not by the acquisition speed of our oscilloscopes. The resulting profiles are shown in Fig. 3B for two measurements, which were taken independently from one another during different round trips of the disc. Measurement points close to the edges of the grooves may suffer from strong scattering and low power levels,

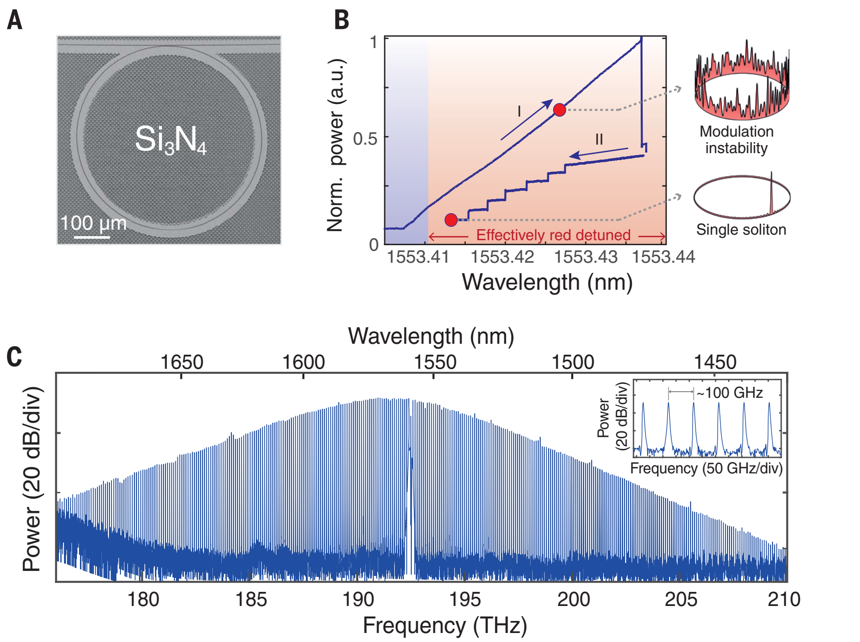

Fig. 1. Dissipative Kerr soliton (DKS) generation in silicon nitride (Si_3N_4) microresonators. (**A**) Scanning electron microscopy image of a silicon nitride microresonator with a radius of 240 μm. The checkerboard pattern results from the photonic Damascene fabrication process (*25*). (**B**) Visualization of the backward tuning technique. The pump laser wavelength is changed from an effective blue-detuning into an effective red-detuned state, thereby increasing the intracavity power and giving rise to modulation instability (arrow I). Eventually, the intracavity field switches from this chaotic state into a multisoliton state when the laser tuning is stopped. From there on, the laser wavelength is tuned toward lower wavelengths, decreasing the number of solitons until a single-soliton state is reached. The decreasing number of solitons is visible by the decreasing steps of the intracavity power (arrow II). (**C**) Spectrum of a DKS optical frequency comb with zoom-in. The spectrum combines large bandwidth and a smooth spectral envelope and features a line spacing of ~100 GHz.

which lead to unreliable distance information. Using the fit error of the linear phase characteristic as a quality criterion, our technique allows identification of such nonusable measurement points and allows automatically discarding them from the data; see (*27*) for details. The raw data of both measurements was further subject to vibrations of the disk arising from the driving engine. These vibrations have been removed by fitting a polynomial to the top surface of the disk and by using it for correction of the overall measurement data. In a first experiment, we analyze the reproducibility of the technique by a detailed comparison of the results obtained from the two measurements (see Fig. 3B, Inset 1). The measured profiles exhibit good agreement regarding macroscopic features such as the groove depth, as well as microscopic features such as surface texture and a decrease of depth toward the edge of the groove. Deviations are attributed to the fact that the two measurements have been taken independently and might hence not have sampled the exact same line across the groove. In addition, we benchmark our technique by comparing the obtained profile of a single groove with a profile obtained from an industrial optical coordinate-measuring machine (CMM, Werth VideoCheck HA) (Fig. 3B, Inset 2). Both profiles are in good agreement, with some minor deviations that we again attribute to slightly different measurement positions along the analyzed groove.

Ultrafast ranging is demonstrated by measuring the profile of a flying air-gun bullet that is shot through the focus of the measurement beam (see Fig. 3C). The projectile moves at a speed of 150 m/s (Mach 0.47), which, together with the acquisition rate of 96.2 MHz, results in a lateral distance of 1.6 μm between neighboring sampling points on the surface of the bullet. The full profile of the projectile is taken during a single shot and depicted in red in Fig. 3D along with a reference measurement obtained from the static bullet using a swept-source optical coherence tomography system (dark blue). For better comparison, the two profiles were rotated and an actual speed of the bullet of 149 m/s was estimated for best agreement. Both curves clearly coincide and reproduce the shape of the fired projectile. Missing data points in the dual-DKS-comb measurement at the tip of the projectile are caused by low power levels of the back-coupled signal, which is inevitable for such steep surfaces in combination with the limited numerical aperture of the lens used for collecting the backscattered light. As before, these measurement points have been discarded from the data based on a large fit error of the linear phase characteristic (*27*). An image of the projectile after recovery from the backstop exhibits a strong corrugation of the bullet toward its back (Fig. 3E). This leads to deviations of the measured profiles in Fig. 3D toward the right-hand side, since the strongly corrugated surface of the projectile in this area has very likely been sampled at two different positions.

To make dual-DKS-comb ranging a viable option for practical applications, the limited ambiguity distance of 1.56 mm must be overcome. This can be achieved, for example, by switching the role of the LO comb and the measurement comb (*6*) or by sending the LO comb also to the target while evaluating not only the difference signal of the balanced photodetectors but also the sum (*28*). Using such techniques,

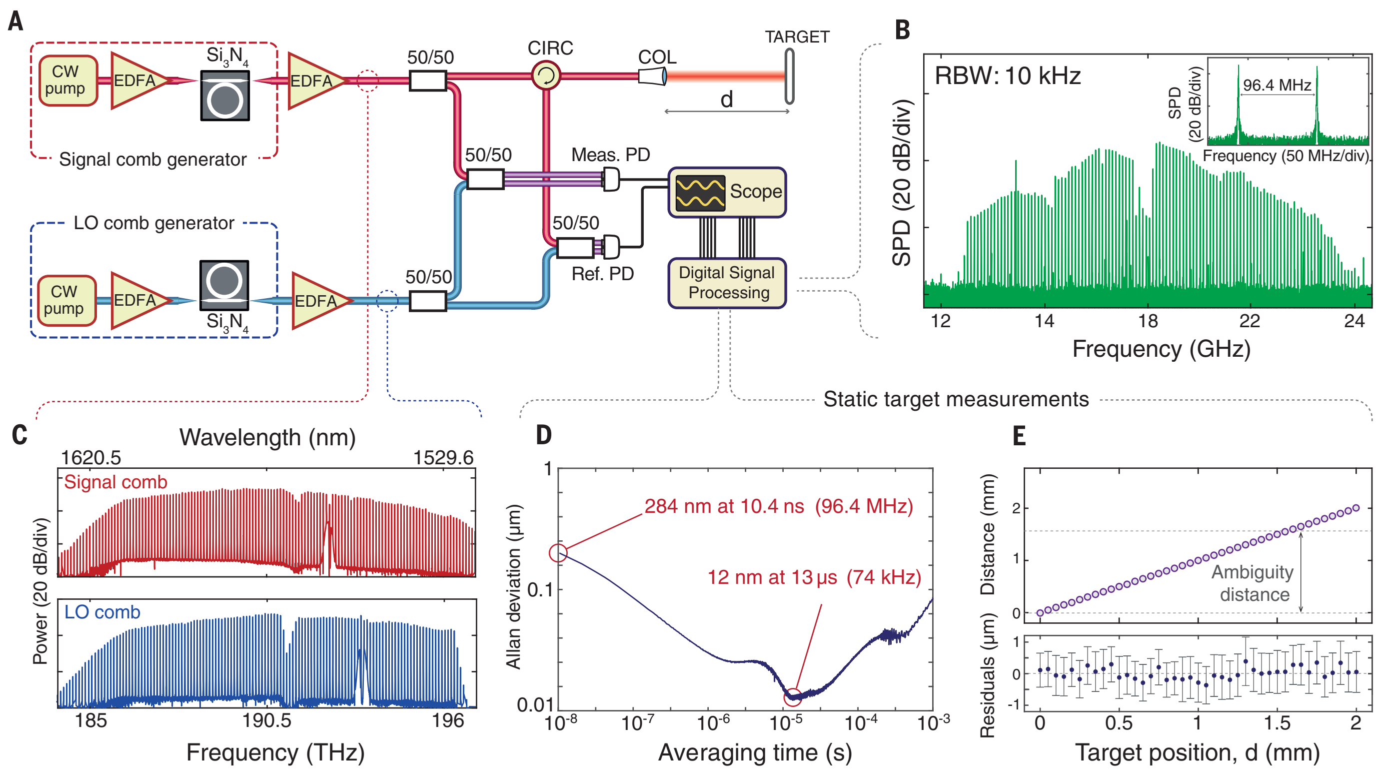

Fig. 2. Experimental demonstration and performance characterization. (**A**) Experimental setup. DKS combs are generated by a pair of silicon nitride (Si_3N_4) microresonators, which are pumped by free-running CW lasers and EDFA. After suppressing residual pump light by fiber Bragg gratings (not shown), the combs are amplified by another pair of EDFA. The signal comb (red) is split, and one part is routed to the target and back to a balanced measurement photodetector (Meas. PD) by optical fibers, an optical circulator (CIRC), and a collimator (COL), while the other part is directly sent to the balanced reference detector (Ref. PD). Similarly, the LO comb is split into two portions, which are routed to the measurement PD and the reference PD for multiheterodyne detection. The resulting baseband beat signals are recorded by a 33-GHz real-time sampling oscilloscope. Digital signal processing is performed offline. (**B**) Numerically calculated Fourier transform of a recorded time-domain signal. (**C**) Optical spectra of the signal comb (red) and the local oscillator comb (blue) after amplification. (**D**) Allan deviation of measured distances as a function of averaging time. The increase toward longer averaging times is attributed to drifts and to mechanical vibrations of the fibers that lead to the target (*27*). (**E**) (Top) Scan of measured position versus set position in steps of 50 μm over the full ambiguity distance (marked by dashed lines). (Bottom) Residual deviations ("residuals") between measured and set positions, with standard deviations as error bars.

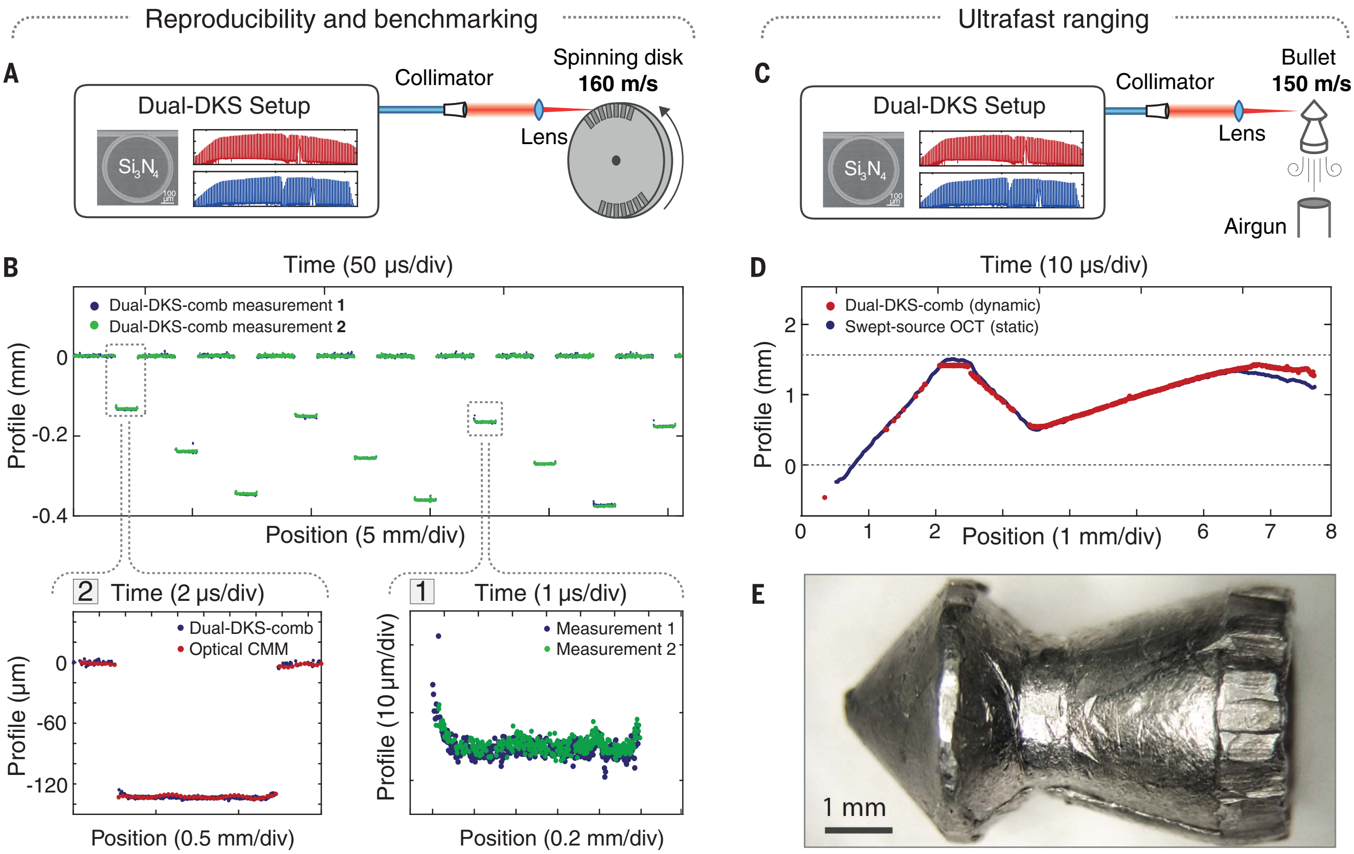

Fig. 3. Reproducibility, benchmarking, and ultrafast ranging demonstration. (**A**) Setup for reproducibility and benchmarking experiments. The measurement beam is focused on the surface of a spinning disk with grooves of different depths. (**B**) Measured surface profile of the disk as a function of position (bottom scale) and time (top scale). The plot contains two independent measurements depicted in blue and green. (Inset 1) Reproducibility demonstration by detailed comparison of the two independent measurements plotted in (B). The measured profiles exhibit good agreement regarding both macroscopic features, such as the groove depth, and microscopic features. (Inset 2) Benchmarking of the high-speed dual-DKS-comb measurement to the results obtained from an industrial optical CMM. (**C**) Setup of ultrafast ranging experiment. (**D**) Measured profile of the projectile obtained from single-shot in-flight dual-DKS-comb measurement (red), along with a swept-source optical coherence tomography (OCT) profile scan that was recorded on the static projectile after recovery from the backstop. The deviations toward the back end of the projectile are attributed to strong corrugations in this area; see (E). (**E**) Image of the projectile after recovery from the backstop.

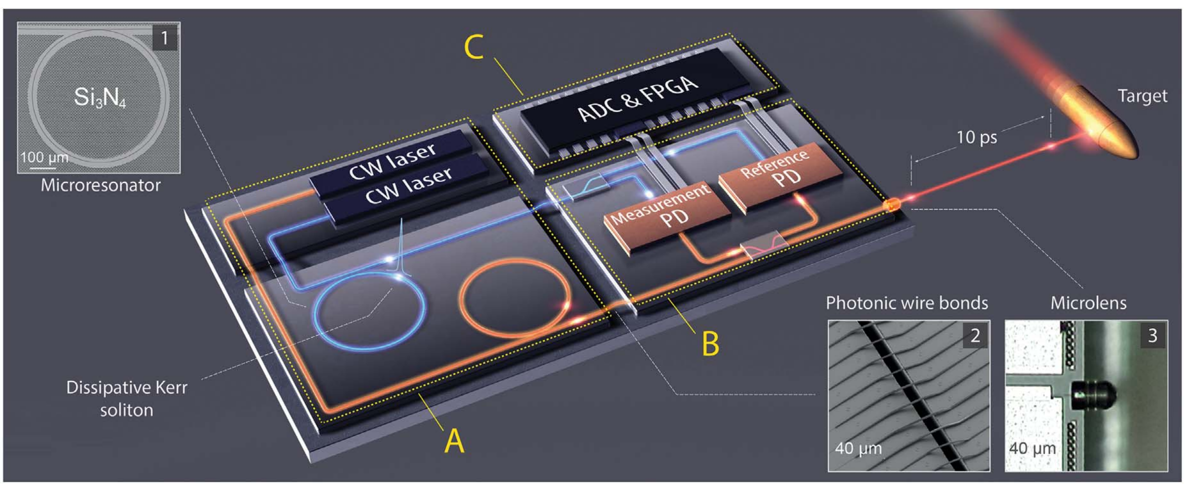

Fig. 4. Artist's view of a dual-comb chip-scale LIDAR engine. The system consists of a dual-frequency comb source (**A**), a photonic integrated circuit (PIC) for transmission and detection of the LIDAR signal (*30*) (**B**), and data acquisition and signal processing electronics (**C**). The system is realized as a photonic multichip assembly that combines the distinct advantages of different photonic integration platforms. The insets show various technologies that could be used to realize the envisioned LIDAR engine. (Inset 1) Si_3N_4 microresonator for comb generation (*24*, *25*). (Inset 2) Photonic wire bonds for chip-chip connections (*29*). (Inset 3) Facet-attached microlens for collimation of the emitted free-space beam (*31*).

high-precision ranging over extended distances should be possible, only limited by coherence lengths of the individual comb lines, which amount to several kilometers. The high acquisition rate allows tracking continuous movements of objects at any practical speed, with an ambiguity limit of ~145,000 m/s.

Our experiments demonstrate the viability of chip-scale DKS comb generators to act as optical sources for high-performance ranging systems and are a key step toward fully integrated chip-scale LIDAR engines, as illustrated as an artist's view in Fig. 4. In this vision, the LIDAR system is realized as a photonic multichip assembly, in which all photonic integrated circuits are connected by photonic wire bonds (Fig. 4, Inset 2) (*29*). The comb generators are pumped by integrated CW lasers, and a dedicated optical chip is used to transmit and receive the optical signals (*30*). The receiver is equipped with a chip-attached microlens that collimates the emitted light toward the target (Fig. 4, Inset 3) (*31*). The electrical signals generated by the photodetectors are sampled by analog-to-digital converters (ADC) and further evaluated by digital signal processing in powerful field-programmable gate arrays (FPGA) or application-specific integrated circuits. Free-running pump lasers greatly simplify the implementation in comparison with configurations where two comb generators are simultaneously pumped by a single light source. Although most of the technological building blocks for realizing this vision have already been demonstrated, one of the remaining key challenges is to reduce the power levels required for DKS generation to typical output power levels of state-of-the-art diode lasers. This requires silicon nitride microresonators with higher quality factors that can be achieved by optimizing the waveguide geometry and the fabrication processes. We expect that such optimizations will allow increasing the Q-factor by about one order of magnitude, thus reducing the pump power requirements by two orders of magnitude. Alternatively, other integration platforms, such as silicon oxide or AlGaAs, can be used, permitting comb generation with only a few milliwatts of pump power (*32*). These power levels are realistically achievable with integrated pump laser diodes. Based on these findings, we believe that DKS-based dual-comb LIDAR could have a transformative impact on all major application fields that require compact LIDAR systems and high-precision ranging, in particular when combined with large-scale nanophotonic phased arrays (*10*, *11*). Acquisition rates of hundreds of megahertz could enable ultrafast three-dimensional imaging with megapixel resolution and update rates of hundreds of frames per second.

REFERENCES AND NOTES

1. M.-C. Amann, T. M. Bosch, M. Lescure, R. A. Myllyla, M. Rioux, *Opt. Eng.* **40**, 1330700 (2001).
2. G. Berkovic, E. Shafir, *Adv. Opt. Photonics* **4**, 441 (2012).
3. T. Udem, R. Holzwarth, T. W. Hänsch, *Nature* **416**, 233–237 (2002).
4. K. Minoshima, H. Matsumoto, *Appl. Opt.* **39**, 5512–5517 (2000).
5. N. Schuhler, Y. Salvadé, S. Lévêque, R. Dändliker, R. Holzwarth, *Opt. Lett.* **31**, 3101–3103 (2006).
6. I. Coddington, W. C. Swann, L. Nenadovic, N. R. Newbury, *Nat. Photonics* **3**, 351–356 (2009).
7. Y.-S. Jang *et al.*, *Sci. Rep.* **6**, 31770 (2016).
8. F. Keilmann, C. Gohle, R. Holzwarth, *Opt. Lett.* **29**, 1542–1544 (2004).
9. V. Ataie *et al.*, *Optical Fiber Communication Conference/ National Fiber Optic Engineers Conference 2013* (2013), p. OTh3D.2.
10. J. Sun, E. Timurdogan, A. Yaacobi, E. S. Hosseini, M. R. Watts, *Nature* **493**, 195–199 (2013).
11. J. C. Hulme *et al.*, *Opt. Express* **23**, 5861–5874 (2015).
12. N. Akhmediev, A. Ankiewicz, *Dissipative Solitons: Lecture Notes in Physics* (Springer, Berlin Heidelberg, 2005).
13. T. Herr *et al.*, *Nat. Photonics* **8**, 145–152 (2013).
14. P. Del'Haye *et al.*, *Nature* **450**, 1214 (2007).
15. T. J. Kippenberg, R. Holzwarth, S. A. Diddams, *Science* **332**, 555 (2011).
16. L. A. Lugiato, R. Lefever, *Phys. Rev. Lett.* **58**, 2209–2211 (1987).
17. W. Liang *et al.*, *Nat. Commun.* **6**, 7957 (2015).
18. J. D. Jost *et al.*, *Optica* **2**, 706 (2015).
19. M.-G. Suh, Q.-F. Yang, K. Y. Yang, X. Yi, K. J. Vahala, *Science* **354**, 600–603 (2016).
20. P. Marin-Palomo *et al.*, *Nature* **546**, 274–279 (2017).
21. D. T. Spencer *et al.*, arXiv:1708.05228 (2017).
22. J. S. Levy *et al.*, *Nature Photonics* **4**, 37 (2010).
23. D. Moss, R. Morandotti, L. Gaeta, M. Lipson *Nat. Photon* **7**, 597 (2013).
24. V. Brasch *et al.*, *Science* **351**, 357–360 (2016).
25. M. H. P. Pfeiffer *et al.*, *Optica* **3**, 20 (2016).
26. H. Guo *et al.*, *Nat. Phys.* **13**, 94–102 (2017).
27. Materials and methods are available as supplementary materials.
28. C. Koos, C. Weimann, J. Leuthold, Multiscale distance measurement with frequency combs, U.S. Patent 20150070685 (2013).
29. N. Lindenmann *et al.*, *Opt. Express* **20**, 17667–17677 (2012).
30. C. Weimann, M. Lauermann, F. Hoeller, W. Freude, C. Koos, *Optics Express* **25**, 30091 (2017).
31. P.-I. Dietrich *et al.*, arXiv:1802.00051 [physics.app-ph] (2018).
32. M. Pu, L. Ottaviano, E. Semenova, K. Yvind, *Optica* **3**, 823–826 (2016).

ACKNOWLEDGMENTS

This work was supported by the Deutsche Forschungsgemeinschaft (DFG) through the Collaborative Research Center "Wave Phenomena: Analysis and Numerics" (CRC 1173, project B3 "Frequency combs"), by the European Research Council (ERC Starting Grant EnTeraPIC, number 280145), by the European Union project BigPipes, by the Alfried Krupp von Bohlen und Halbach Foundation, by the Karlsruhe School of Optics and Photonics (KSOP), and by the Helmholtz International Research School for Teratronics (HIRST). D.G. is supported by the Horizon 2020 Research and Innovation Program under the Marie Sklodowska-Curie grant agreement no. 642890 (TheLink). P.M.-P. is supported by the Erasmus Mundus doctorate program Europhotonics (grant number 159224-1-2009-1-FR-ERA MUNDUS-EMJD). Si_3N_4 devices were fabricated and grown in the Center of MicroNanoTechnology (CMi) at EPFL. EPFL acknowledges support by the U.S. Air Force Office of Scientific Research, Air Force Material Command, USAF, number FA9550-15-1-0099. This work is supported by the European Space Technology Centre with ESA contract no. 4000116145/16/NL/MH/GM. This work was supported by funding from the Swiss National Science Foundation under grant agreement no. 161573 (precoR). The data sets are available through Zenodo at https://doi.org/10.5281/zenodo.1116280.

SUPPLEMENTARY MATERIALS

www.sciencemag.org/content/359/6378/887/suppl/DC1
Materials and Methods
Figs. S1 to S6
Table S1
References (*33*–*36*)

17 July 2017; accepted 11 January 2018
10.1126/science.aao3924

Science

Ultrafast optical ranging using microresonator soliton frequency combs

P. Trocha, M. Karpov, D. Ganin, M. H. P. Pfeiffer, A. Kordts, S. Wolf, J. Krockenberger, P. Marin-Palomo, C. Weimann, S. Randel, W. Freude, T. J. Kippenberg and C. Koos

Science **359** (6378), 887-891.
DOI: 10.1126/science.aao3924

Miniaturized optical ranging and tracking

Light detection and ranging systems are used in many engineering and environmental sensing applications. Their relatively large size and cost, however, tend to be prohibitive for general use in autonomous vehicles and drones. Suh and Vahala and Trocha *et al.* show that optical frequency combs generated by microresonator devices can be used for precision ranging and the tracking of fast-moving objects. The compact size of the microresonators could broaden the scope for widespread applications, providing a platform for miniaturized laser ranging systems suitable for photonic integration.

Science, this issue p. 884, p. 887